

Electroosmotic Flow in Composite Microchannels and Implications in Microcapillary Electrophoresis Systems

F. Bianchi,[†] F. Wagner,[‡] P. Hoffmann,[‡] and H. H. Girault^{*.†}

Laboratoire d'Electrochimie and Institut d'Optique Appliquée, Ecole Polytechnique Fédérale de Lausanne, CH-1015 Lausanne, Switzerland

The electroosmotic flow in laminated excimer laser-ablated microchannels has been studied as a function of the depth of the rectangular channels, and particular emphasis has been given to the difference in the ζ -potentials between the lamination layer and the ablated substrate. Experimental electroosmotic flow follows the tendency predicted by a recently published model. The ζ -potentials of lamination and ablated surfaces were determined for poly(ethylene terephthalate) and poly(carbonate) substrates by fitting the experimental data with a numerical implementation of this model. In the experimentally investigated range of channel cross sections, a linear fit to the data gives a good approximation of the ζ -potentials for both materials. Moreover, a flow injection analysis of fluorescein dye has been performed to show the severe loss in numbers of theoretical plates, caused by Taylor dispersion, when such microchannels, dedicated to microcapillary electrophoresis, are used.

Ultraviolet laser ablation has been shown to be a powerful tool for machining structures in the micrometer range, using organic polymer substrates.^{1–4} More recently, this technique has been applied to the fabrication of microchannels,^{5,6} giving a promising way to produce microdevices for performing microscale flow injection analysis (μ -FIA),^{7–12} as an intermediate step toward the concept of microscale total analysis systems (μ -TAS).^{6,13–16}

Different channel dimensions and geometries can be easily obtained by varying UV laser ablation parameters: substrate translation speed ($1–10^5 \mu\text{m/s}$), laser fluence ($30–2500 \text{ mJ/cm}^2$), pulse repetition rate ($1–50 \text{ Hz}$), and the mask shape. A low-temperature lamination technique allows the closing of the channel, and the final structure exhibits electroosmotic properties similar to those of microchannels produced in silicon or fused silica substrates.⁵

Electroosmotic pumping, generated by means of an external electrical field, has been demonstrated as a suitable way to drive successfully nanovolumes, within microcapillary electrophoresis (μ -CE) systems, as a valveless system.^{8,17–22} However, several studies^{23–27} on fluid dynamics induced by electroosmotic flow (EOF) in microfabricated devices have pointed out an unexpected behavior, that the simple Smoluchowski model cannot predict. Most of the microscale fabrication processes used to produce microchannels result in channels having geometry and/or materials composition differing considerably from those of the silica capillaries used in a conventional electrophoretic apparatus.^{17,21,28}

[†] Laboratoire d'Electrochimie.

[‡] Institut d'Optique Appliquée.

- (1) Seddon, B. J.; Shao, Y.; Fost, J.; Girault, H. H. *Electrochim. Acta* **1994**, *39*, 783–791.
- (2) Seddon, B. J.; Shao, Y.; Girault, H. H. *Electrochim. Acta* **1994**, *39*, 2377–2386.
- (3) Lazare, S.; Drillhole, D. J. *Photochem. Photobiol. A—Chem.* **1997**, *106*, 15–20.
- (4) Ho, C. K.; Man, H. C.; Yue, T. M.; Yuen, C. W. *Appl. Surf. Sci.* **1997**, *110*, 236–241.
- (5) Roberts, M. A.; Rossier, J. S.; Bercier, P.; Girault, H. *Anal. Chem.* **1997**, *69*, 2035–2042.
- (6) Schwarz, A.; Rossier, J. S.; Bianchi, F.; Reymond, F.; Ferrigno, R.; Girault, H. H. In *Micro Total Analysis Systems '98*; Harrison, D. J., van den Berg, A., Eds.; Kluwer Academic Publishers: Dordrecht/Boston/London, 1998; pp 241–244.
- (7) Rossier, J. S.; Schwarz, A.; Reymond, F.; Ferrigno, R.; Bianchi, F.; Girault, H. H. *Electrophoresis* **1999**, *20*, 727–731.
- (8) Harrison, D. J.; Fluri, K.; Seiler, K.; Fan, Z. H.; Effenhauser, C. S.; Manz, A. *Science* **1993**, *261*, 895–897.
- (9) Hadd, A. G.; Jacobson, S. C.; Ramsey, J. M. *Anal. Chem.* **1999**, *71*, 5206–5212.

- (10) Woolley, A. T.; Mathies, R. A. *Anal. Chem.* **1995**, *67*, 3676–3680.
- (11) Haswell, S. J. *Analyst* **1997**, *122*, R1–R10.
- (12) Effenhauser, C. S. *Top. Curr. Chem.* **1998**, *194*, 51–82.
- (13) Manz, A.; Verpoorte, E.; Raymond, D. E.; Effenhauser, C. S.; Burggraf, N.; Widmer, H. M. In *Micro Total Analysis Systems*; van den Berg, A., Bergveld, P., Eds.; Kluwer Academic Publishers: Dordrecht, 1995.
- (14) Dempsey, E.; Diamond, D.; Smyth, M. R.; Urban, G.; Jobst, G.; Moser, I.; Verpoorte, E. M. J.; Manz, A.; Widmer, H. M.; Rabenstein, K.; Freaney, R. *Anal. Chim. Acta* **1997**, *346*, 341–349.
- (15) Shoji, S. *Top. Curr. Chem.* **1998**, *194*, 163–188.
- (16) Vandenberg, A.; Lammerink, T. S. J. *Top. Curr. Chem.* **1998**, *194*, 21–49.
- (17) Harrison, D. J.; Manz, A.; Fan, Z. H.; Ludi, H.; Widmer, H. M. *Anal. Chem.* **1992**, *64*, 1926–1932.
- (18) Harrison, D. J.; Glavina, P. G.; Manz, A. *Sens. Actuators B* **1993**, *10*, 107–116.
- (19) Li, P. C. H.; Harrison, D. J. *Anal. Chem.* **1997**, *69*, 1564–1568.
- (20) Jacobson, S. C.; Hergenroder, R.; Koutny, L. B.; Ramsey, J. M. *Anal. Chem.* **1994**, *66*, 1114–1118.
- (21) Jacobson, S. C.; Moore, A. W.; Ramsey, J. M. *Anal. Chem.* **1995**, *67*, 2059–2063.
- (22) Seiler, K.; Fan, Z. H. H.; Fluri, K.; Harrison, D. J. *Anal. Chem.* **1994**, *66*, 3485–3491.
- (23) Bianchi, F.; Ferrigno, R.; Girault, H. H. *Anal. Chem.* **2000**, *72*, 1987–1993.
- (24) Culbertson, C. T.; Jacobson, S. C.; Ramsey, J. M. *Anal. Chem.* **1998**, *70*, 3781–3789.
- (25) Culbertson, C. T.; Ramsey, R. S.; Ramsey, M. J. *Anal. Chem.* **2000**, *72*, 2285–2291.
- (26) Andreev, V. P.; Dubrovsky, S. G.; Stepanov, Y. V. *J. Microcolumn Sep.* **1997**, *9*, 443–450.
- (27) Hadd, A. E.; Molho, J. I.; Santiago, J. S.; Mungal, M. J.; Kenny, T. W. *Anal. Chem.* **2000**, *72*, 1053–1057.

In a recent report, Andreev et al.²⁶ modeled the EOF in microchannels with rectangular cross sections and different ζ -potentials on the walls and showed that the shape of the electroosmotic flow velocity profile differs from the usual flat plug flow profile. It has been shown that this flow particularity results in a loss of resolution due to Taylor dispersion,²⁹ if such composite microchannels are used to perform electrokinetically driven separations.

In the present paper we report experimental results for the EOF in two kinds of composite microchannels made of poly(ethylene terephthalate)–polyethylene (PET–PE) and poly(carbonate)–polyethylene (PC–PE) substrates, obtained by UV laser ablation and a lamination technique. The mathematical model of ref 26 is numerically implemented in order to analyze the experimental data. From these studies, the ζ -potentials of the materials composing the microstructure are determined. With similar channel structures, simple microscale flow injections of fluorescein dye are used to study the effect of Taylor dispersion on the peak broadening.

EXPERIMENTAL SECTION

1. Prototyping Procedure. The microstructures were fabricated using ArF excimer laser ablation at 193 nm and a low-temperature lamination technique.⁵ We used two types of polymer films as substrates: (i) PET-Melinex (grade S), ICI, UK (thickness 100 μm), and (ii) PC-Makrolon (grade D1), Goodfellow, UK (thickness 125 μm). The substrates were placed on computer-controlled X – Y translation stages (Physik Instrumente, Germany) and scanned under the excimer laser beam (Lambda Physik LPX 205-i) during the ablation procedure.

The ablation setup was a standard mask projection setup, where the image of a free-standing molybdenum mask with a rectangular hole is projected on the substrate. For the production of channels with different depths, the laser is operated with constant parameters (pulse repetition rate, 50 Hz; fluence, 850 mJ/cm^2), and the substrate is scanned with different speeds (100–400 $\mu\text{m}/\text{s}$) under the beam. The 2-cm-long channels were 50 μm wide in all cases, and the channel depth varied between 15 and 60 μm due to the different scan velocities. The structure dimensions (widths and depths, Figure 1) were measured with an inspection and 2-D metrology microscope coupled with a digital camera (Nikon Coolpix).

Prior to sealing of the structure by using a lamination machine (Morane Senator, Oxon, UK), the channels were first rinsed with 2-propanol (Fluka, Switzerland) and distilled water in order to remove weakly adherent debris resulting from the ablation process.^{30,31} After being rinsed, the samples were dried in a nitrogen gas stream.

2. Electroosmotic Flow Measurements. The influence of the inhomogeneous ζ -potential distribution on the flow behavior is observed by measuring the average EOF velocity in a set of microchannels, differing only in depth. This permits the discrimination of the contributions of each material to the electroosmotic flow.

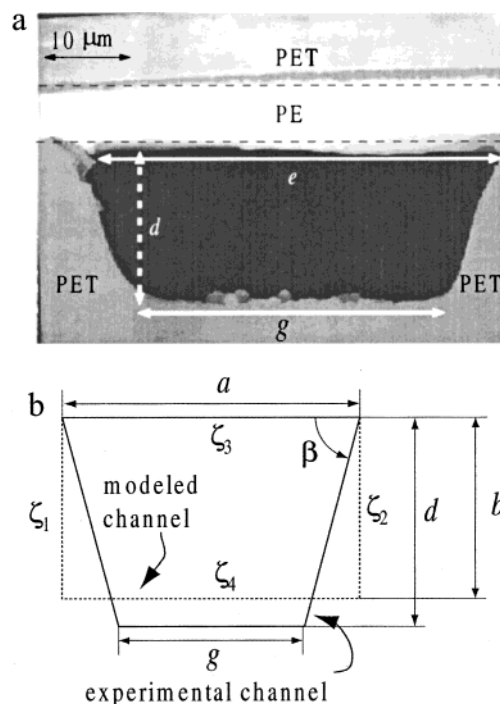


Figure 1. (a) SEM micrograph of a cross section of an excimer laser-ablated polymer microchannel. The capillary walls are composed of PE from the lamination sheet (top side) and photoablated PET (bottom and lateral sides). The different lengths measured to define the section of the channel are g , d , and e . (b) Schematic diagram of the modeled channel. For all calculations, $\zeta_1 = \zeta_2 = \zeta_4 = \zeta_a$ and $\zeta_3 = \zeta_i$.

The electroosmotic flow velocity in the channels, averaged over the whole cross section, is measured using Huang's method.³² We follow Roberts's experimental procedure⁵ to monitor the current evolution as a function of time using a high-voltage power supply (CZE1000R Spellman) interfaced to a multifunction analog, digital, and timing input/output board (PCI-1200, National Instruments). The microchannels are mounted horizontally, and the volume in the two reservoirs is kept constant to prevent pressure effects. To avoid already observed aging influences, the microchannels for one set of experiments are fabricated on the same day, and the EOF measurements are carried out with freshly prepared buffer solutions. We used buffer concentrations of 15 and 12 mM acetate buffer, pH 4.66 (acetic acid 0.1 M, sodium acetate 0.1 M, Merck). Further, we have chosen to work with a low operating electric field, 200 V/cm, to allow accurate heat dissipation. Hence, the transversal gradient in viscosity is minimized, and thermal effects on the EOF can be neglected.³³

3. Flow Injection Analysis. A flow injection analysis has been performed to determine the separation efficiency of the photoablated composite microchannels using an experimental approach similar to the pioneering works achieved by Jacobson et al.^{20,34} and Effenhauser et al.³⁵ A schematic representation of the microchip used for injection analysis is presented in Figure 2a. Briefly, the microchannels are filled with a buffer solution by

(28) Rodriguez, I.; Zhang, Y.; Lee, H. K.; Li, S. F. Y. *1997*, 781, 287–293.

(29) Taylor, G. I. *Proc. R. Soc. London* **1953**, A219, 186–203.

(30) Rossier, J. S.; Bercier, P.; Schwarz, A.; Loridant, S.; Girault, H. H. *Langmuir* **1999**, 15, 5173–5178.

(31) Wagner, F.; Hoffmann, P. *Appl. Phys. A (Suppl.)* **1999**, 69, s841–s844.

(32) Huang, X.; Gordon, M. J.; Zare, R. N. *Anal. Chem.* **1988**, 60, 1837–1838.

(33) Knox, J. H. *Chromatographia* **1988**, 26, 329–337.

(34) Jacobson, S. C.; Hergenroder, R.; Koutny, L. B.; Warmack, R. J.; Ramsey, J. M. *Anal. Chem.* **1994**, 66, 1107–1113.

(35) Effenhauser, C. S.; Manz, A.; Widmer, H. M. *Anal. Chem.* **1993**, 65, 2637–2642.

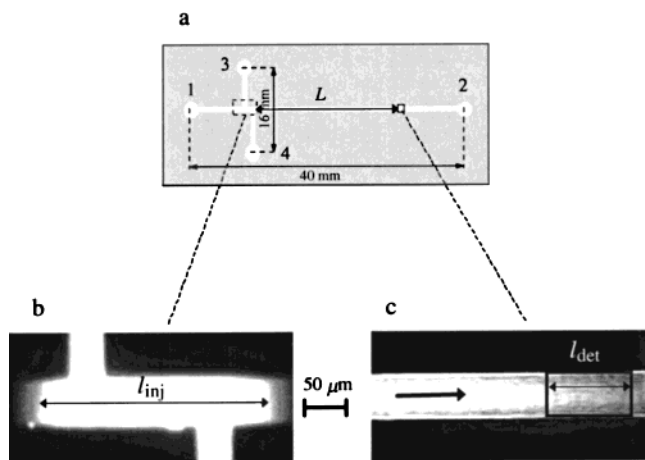


Figure 2. (a) Schematic representation of the microchip used for the flow injection analysis with the following reservoirs: (1) buffer reservoir, (2) waste reservoir, (3) sample reservoir, and (4) sample waste reservoir. The separation length L has been set at six different values for the different injection analysis, from 0.5 to 4 cm. (b) Fluorescence image during double T-injection; the length l_{inj} is defined not only by the structure dimensions but also by the diffusion coefficient D combined with the injection time. Keeping for all experiments the same injection time, the injection length, l_{inj} , is constant and its value is about $275 \mu\text{m}$. (c) Fluorescence detection of the plug arriving at the detection window, which is fixed by the digital processing described in the Experimental Section. The length of the detection window is $l_{det} = 100 \mu\text{m}$.

capillary flow. All reservoirs contain $150 \mu\text{L}$ of buffer solution except reservoir 3, which is filled with the sample solution. Fluorescein salt is purchased from Fluka (Buchs, Switzerland), and the sample dilution ($50 \mu\text{M}$) is performed in alkaline medium, pH 9.2 buffer (20 mM sodium tetraborate, Fluka), to increase the fluorescence signal.³⁶

Applying a voltage between reservoirs 3 (0.8 kV) and 4 (ground), and letting the electrodes in reservoirs 1 and 2 float, causes the sample solution to be pumped in the injection part of the device (floating procedure³⁵) (Figure 2b). During the separation a pullback procedure^{34,37} is applied, preventing sample leakage from the sidearm channels into the separation channel. The voltage is applied between reservoirs 1 (2 kV), 3 (0.5 kV), 4 (0.5 kV), and 2 (ground), inducing flow of buffer solution from 1 to 3, 1 to 4, and 1 to 2 (Figure 2c).

The fluorescence detection and microscopic investigation are performed using a confocal microscope (Axiovert 25, lamp HPO 100 W, Zeiss) with a highly sensitive CCD black-and-white camera (CF 8/4, Kappa, Germany) interfaced to an 8-bit flash analog-to-digital converter (ADC) monochrome IMAQ board (PCI-1408, National Instruments). During the separation, the image data are grabbed (24 frames/s) only in the detection window (Figure 2c) and directly converted into an intensity histogram by digital processing, using Imaq Vision for program Labview (National Instruments). The program also allows the characterization of the lengths l_{inj} of the injected volume and l_{det} of the detection window (see Figure 2b,c), which are $l_{inj} = 275 \mu\text{m}$ and $l_{det} = 100 \mu\text{m}$, respectively.

(36) Yeung, E. S.; Khur, W. G. *Anal. Chem.* **1991**, *63*, 275A.

(37) Ermakov, S. V.; Jacobson, S. C.; Ramsey, J. M. *Anal. Chem.* **2000**, *72*, 3512–3517.

THEORY

1. Mathematical Model. The mathematical considerations are based on the model reported by Andreev et al.²⁶ Here, we present the assumptions made in this work and give the equations which describe the electroosmotic flow in channels of rectangular cross section, where every channel wall may exhibit a different ζ -potential.

The calculation is based on the assumptions listed below.

1. Capillary end effects are neglected; i.e., the transverse capillary dimensions, a and b (see Figure 1b), are considered to be much shorter than the channel length.

2. Thermal effects are not taken into consideration.

3. ζ -potentials are considered to be homogeneous along the longitudinal coordinate.

4. The buffer is considered to be a univalent electrolyte.

According to Rice and Whitehead,³⁸ in assumption 4, the Debye–Hückel approximation, (e.g., the linearization of the Poisson–Boltzmann equation) can be used even for ζ -potentials up to 50 mV. With a methodology similar to that presented in a former report,²³ the Poisson–Boltzmann equation for electrical potential φ and charge distribution ρ_e is inserted in the Navier–Stokes equation, with the following boundary conditions:

$$\begin{aligned} \varphi(0, y) &= \zeta_2 & \varphi(x, 0) &= \zeta_4 \\ \varphi(a, y) &= \zeta_1 & \varphi(x, b) &= \zeta_3 \end{aligned} \quad (1)$$

where x and y are transverse coordinates and ζ_1 , ζ_2 , ζ_3 , and ζ_4 the ζ -potentials of the channel walls, represented in Figure 1b.

The analytical solution presented by Andreev et al. for the electroosmotic flow profile $v(x, y)$ is then

$$\begin{aligned} v(x, y) = & \frac{-4b_0^2}{\pi} \left\{ \sum_{k=0}^{\infty} \frac{\sin(p_k y)}{2k+1} \left(\zeta_1 \left[\frac{\sinh(p_k x)}{\sinh(p_k a)} - \frac{\sinh(q_k x)}{\sinh(q_k a)} \right] + \right. \right. \\ & \left. \left. \zeta_2 \left[\frac{\sinh(p_k(a-x))}{\sinh(p_k a)} - \frac{\sinh(q_k(a-x))}{\sinh(q_k a)} \right] \right) \right\} + \\ & \sum_{k=0}^{\infty} \frac{\sin(m_k x)}{2k+1} \left\{ \zeta_3 \left[\frac{\sinh(m_k y)}{\sinh(m_k b)} - \frac{\sinh(n_k y)}{\sinh(n_k b)} \right] + \right. \\ & \left. \left. \zeta_4 \left[\frac{\sinh(m_k(b-y))}{\sinh(m_k b)} - \frac{\sinh(n_k(b-y))}{\sinh(n_k b)} \right] \right) \right\} \end{aligned} \quad (2)$$

where $b_0^2 = \epsilon E / \eta$, ϵ and η are respectively the permittivity and the viscosity of bulk electrolyte, E is the electric field strength along the capillary, and

(38) Rice, C. L.; Whitehead, R. *J. Phys. Chem.* **1965**, *69*, 4017–4024.

$$\begin{aligned}
 p_k &\equiv \frac{\pi(2k+1)}{b} & q_k &\equiv \sqrt{p_k^2 + \kappa^2} \\
 m_k &\equiv \frac{\pi(2k+1)}{a} & n_k &\equiv \sqrt{m_k^2 + \kappa^2}
 \end{aligned}
 \quad (3)$$

where κ^{-1} is the Debye length.

2. Application to Ablated Channels. Equation 2 applies to rectangular channels where each side of the channel is allowed to have a different ζ -potential. However, the ablated channels are composed of only two different materials (Figure 1b): PE top cover from the PE–PET lamination sheet closing the channel and three photoablated PET or PC walls, from the PET or PC substrate. The ζ -potential of the three ablated surfaces is determined by well-adherent debris,³⁹ which is the same for the channel floor and the channel walls. Thus, the ablated surfaces have approximately the same ζ -potential, ζ_a . In eq 2 we use then $\zeta_1 = \zeta_2 = \zeta_4 = \zeta_a$, and $\zeta_3 = \zeta_l$ is the value of the ζ -potential of the lamination.

The ablated channels have a trapezoidal cross section (Figure 1b) where the angle of the sidewalls is about 70°. For all produced channels, the upper width e , the lower width g , and the channel depth d have been determined. Hence, the fraction e/f of the lamination with respect to the total section perimeter f is given by

$$e/f = e / \left(e + g + 2 \sqrt{\left(\frac{e-g}{2}\right)^2 + d^2} \right) \quad (4)$$

where the different lengths are defined in Figure 1b. The rectangular channel that is used in the calculation (dashed line) then has the width $a = e$ and the depth $b = 1/2(f - 2a)$, in order to give the same value of e/f . Consequently, the channel in the calculations is slightly shallower than the experimental one (Figure 1b).

3. Numerical Implementation. As eq 2 contains infinite series that cannot be evaluated symbolically, the implementation of eq 2 is numerical. This means simply that the sums are not evaluated to infinity but up to $k = k_{\text{up}}$. The experimental value of the electroosmotic measurements is the average stream velocity of the liquid in the channel v_{av} . To obtain this value from eq 2, one needs to integrate the velocity profile over the whole channel cross section:

$$v_{\text{av}} = \frac{1}{ab} \int_{x=0}^a \int_{y=0}^b v(x,y) \, dy \, dx \quad (5)$$

Because of the numerical evaluation of eq 2, this integral is necessarily also numerical. Hence,

$$v_{\text{av}}(e/f, \zeta_a, \zeta_l) = \frac{1}{N_x N_y} \sum_{i=1}^{N_x} \sum_{j=1}^{N_y} v(x_i, y_j) \quad (6)$$

(39) Wagner, F.; Hoffmann, P. *Proc. SPIE-Int. Soc. Opt. Eng.* **2000**, 4088, 322–325.

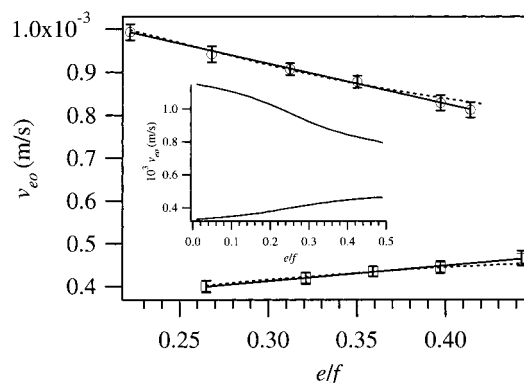


Figure 3. Experimental values of the average electroosmotic flow velocity at pH 4.6 in PET–PE and PC–PE microchannels as a function of the ratio e/f (lamination distance/total cross section perimeter). Full and dashed lines represent respectively linear and eqs 2 and 6 fits; respective errors of this fits are given in Table 1. The inset shows the theoretical curve, for the PE–PET and PE–PC microchannels, calculated with the implementation of the mathematical model, over nearly the whole range of possible e/f values.

where the parameters N_x and N_y are the number of cells for the numerical integration. The x_i and y_j are spaced equidistant from 0 to a and b , respectively.

Variation of k_{up} results in variations in the average velocity v_{av} only if $k_{\text{up}} < 50$. Usually we used a value of $k_{\text{up}} = 200$. The variations in v_{av} due to variations of the grid size $N_x \times N_y$ become negligible for a grid size of more than 300×300 points.

Even when using a 10-byte data type (maximum 1.1×10^{4932}) for the implementation of eqs 2 and 6, overflow occurs in the sinh term in eq 2 when a realistic value for the Debye length is used ($\kappa^{-1} \approx 3$ nm). Approximations of the fractions, indicated by the numbers 1–8 in eq 2, have to be used in order to avoid this. The fractions 1, 2, 5, and 6 in eq 2 are of the form $\sinh(c_1 x) / \sinh(c_1 c_2)$ (c_1 and c_2 are constants) and can be approximated by $\exp(c_1(x - c_2))$ for $c_1 \gg c_2, x$. The fractions 3, 4, 7, and 8 in eq 2 are of the form $\sinh(c_1(c_2 - x)) / \sinh(c_1 c_2)$ and can be approximated by $\exp(c_1 x)$ if $c_1 \gg c_2, x$. If underflow occurs in the approximation terms, the fraction is set to 0. In this form, $v_{\text{av}}(e/f, \zeta_a, \zeta_l)$ is used as fit function to the experimental data in order to determine the ζ -potentials of the lamination and the ablated surface.

ELECTROOSMOTIC FLOW

In Figure 3, the measured electroosmotic flow velocities, v_{eo} , in two different microstructures are reported as a function of the ratio e/f . Each experimental point (round and square markers in Figure 3) represents the average value of 14 consecutive EOF measurements described in the Experimental Section. The error bars in Figure 3 are the relative standard deviation (RSD) around v_{eo} . For all measurements, the EOF in the microchannels for PET as substrate is higher than that for PC as substrate, as previously illustrated by Roberts et al., at pH 7.2.⁵ The variations of EOF as functions of microchannel dimensions have not been demonstrated yet.

In a conventional capillary, which is made from only one material, the electroosmotic flow velocity is independent of the capillary dimensions as long as the diameter is considerably larger than the double-layer thickness.⁴⁰ In this case, the electroosmotic flow velocity v_{eo} is described by the Schmoluchowsky equation:

Table 1. ζ -Potentials (mV) at pH 4.6 Obtained from the Fit of Experimental Data with (i) a Linear Combination of the Smoluchowski Equation and (ii) a Numerical Implementation of Eqs 2 and 6^a

	linear fits		fits from eqs 2 and 6	
	from PET–PE	from PC–PE	from PET–PE	from PC–PE
ζ_{PET}	-87 ± 2		-84 ± 3	
ζ_{PC}	-22 ± 4		-24 ± 2	
ζ_{PE}	-19 ± 3	-48 ± 2	-32 ± 4	-44 ± 3

^a The errors are the standard deviations of the fitting parameters.

$$v_{\text{eo}} = -\frac{\epsilon \zeta E}{\eta} \quad (7)$$

where ζ represents the ζ -potential of the capillary wall and the other parameters are as in eq 2.

However, in laminated channels, the experimental data clearly show a dependence on the ratio e/f (see Figure 3). Within the investigated range for e/f the electroosmotic velocity decreases for PET–PE microchannels from 1 mm/s with increasing e/f to 0.82 mm/s, while the tendency for PC–PE microchannel is less pronounced and opposite in sign. Here, the EOF increases with increasing e/f from 0.4 to 0.45 mm/s. From these results, the subsequent relation (eq 8) can classify the ζ -potentials, because of the relative contribution of each material to the electroosmosis.

$$|\zeta_{\text{PET}}| > |\zeta_{\text{PE}}| > |\zeta_{\text{PC}}| \quad (8)$$

The linear fits, presented in Figure 3 (full line), show a good agreement with measured EOF for both microchannels types. A first approach, to obtain the ζ -potentials of the two wall materials from the measured average EOF velocities v_{av} , is thus a linear combination of the Smoluchowski equations (eq 9) of both wall materials:

$$v_{\text{av}} \approx \frac{E\epsilon}{\eta} [(e/f)\zeta_1 + (1 - (e/f))\zeta_a], \quad \text{for } 0.22 < e/f < 0.44 \quad (9)$$

Combining the fitting parameters, the slope m , and the origin ordinate n , in eq 9, gives the values of the ζ -potentials presented in Table 1. Using eq 9 for the determination of the ζ -potentials represents, however, an extrapolation of the linear relationship, which is not allowed. For example, the determination of the origin ordinate n corresponds to the extrapolation of eq 9 to values of $e/f \cong 0$, i.e., very deep channels. Nevertheless, it is clear that the electroosmotic flow velocity in very deep channels is constant, because the influence of the lamination is negligible. This extrapolation problem shows up clearly when comparing the ζ -potentials of the lamination, ζ_{PE} , obtained from the two different channel types (PET–PE and PC–PE). In both channel types the same lamination was used, and thus the two values of ζ_{PE} should be identical (within the error). As a result of the extrapolation, however, the values differ by more than 60% (Table 1). Therefore, it can be deduced that the linear model is not good enough to

determine the ζ -potentials. Consequently, it is important to note that the validity of eq 9, i.e., the linearity of $v_{\text{av}}(e/f)$, is restricted to a certain range of e/f values. In the inset graph, presented in Figure 3, the plots of eq 6 show clearly that the tendency of the electroosmotic flow in a larger domain of e/f ($0 < e/f < 0.5$) deviates from linearity.

To obtain more accurate values on the ζ -potentials, eq 6 is implemented as a fitting function. The ζ -potentials ζ_a and ζ_l are used as fitting parameters, and the other numerical parameters are fixed ($k_{\text{up}} = 200$, $N_x N_y = 200 \times 300$). The resulting curves are presented as function of the ratio e/f in Figure 3 (dashed lines), and the resulting ζ -potentials (fit parameters) are also presented in Table 1. The results of this nonlinear fitting method agree completely with relation (8), which was not the case for the extrapolated linear fit. Further, the two values for ζ_{PE} , which were once more obtained by fitting independently the PET–PE and the PC–PE channel data, are much closer together than for the extrapolated linear fit (now 27% deviation instead of 60% before). The nonlinear fit thus allows a better estimation of the ζ -potentials.

However, even with the nonlinear fitting method, the two values for ζ_{PE} are not identical within their errors. The remaining difference can be attributed partly to the experimental error (that is, approximately 10%) and partly to the assumptions presented in the Theory section. Particularly, the Debye–Hückel approximation is valid for ζ -potential values up to 50 mV, which is not the case for the ζ -potential value of photoablated PET (see Table 1). Moreover, the rectangular section in the mathematical model does not describe properly the trapezoidal section of the experimental channels (Figure 1b). These effects will both influence the value of ζ_{PE} . The standard deviations of the fitting parameters are given in Table 1, and the precision of the ζ -potential determination can be enhanced in the future by using more data points. A quantitative statistical comparison of the two fitting methods would only be possible after fitting with each method simultaneously the data for both channel types using three fit parameters (ζ_{PET} , ζ_{PC} , and ζ_{PE}). Evaluating the quantitative influence of the rectangular approximation of the trapezoidal microchannel cross section and the validity of the Debye–Hückel approximation would require a comparison of the presented results with a numerical solution of the fundamental equations (Poisson–Boltzmann equation, Navier–Stokes equation) within the boundary conditions of a trapezoidal microchannel. However, this exceeds the aim of this article.

Despite the remaining uncertainties, the nonlinear fit gives exploitable ζ -potential values, which allow for the visualization of the electroosmotic flow velocity profile in the studied microcomposite channels. In Figure 4, two-dimensional electroosmotic flow velocity profiles $v(x,y)$ are plotted using the numerical implementation of eq 2 and the ζ -potential values from Table 1 (right side). Strong deviations from the flat plug profile (Figure 4a) are observed in Figure 4b,c, as has been already demonstrated with cross sections of $v(x,y)$ presented by Andreev et al.²⁶

PEAK BROADENING

A disparity in the ζ -potentials between materials composing a microchannel has been predicted to cause a severe loss in the resolution R_s of the capillary electrophoresis system, due to Taylor dispersion.²⁶ In Figure 5a, four fluorescence detection peaks (dots) of a fluorescein salt are shown. They have been recorded

(40) Tsuda, T.; Nomura, K.; Nakagawa, G. *J. Chromatogr.* **1982**, *248*, 241–247.

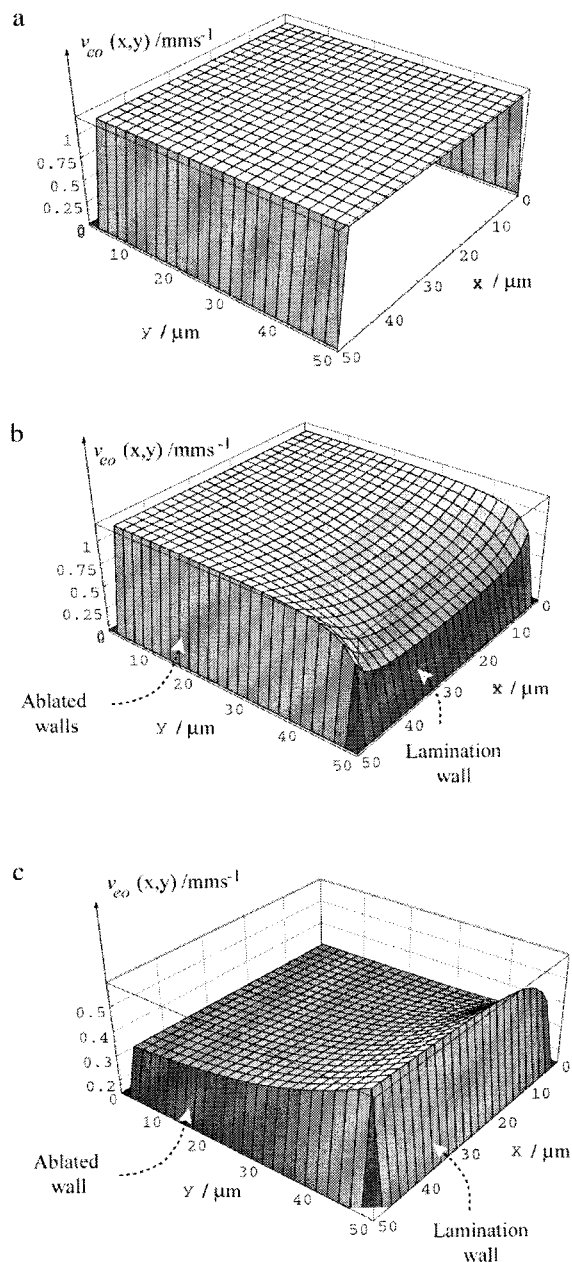


Figure 4. Calculated 2D electroosmotic flow velocity profiles $v(x,y)$, (a) with homogeneous ζ -potential (ζ_a), (b) featuring PET-PE microchannels, and (c) featuring PC-PE microchannels. The ζ -potential values were taken from Table 1 (right side). The right side in front is the side with the lamination. The three other sides are ablated.

subsequently at the same detection place and illustrate the excellent reproducibility of this measurement. Fitting the experimental results with an asymmetric peak function (eq 10) (dashed line) gives a correlation value of $R^2 = 0.9991$, rather than the gauss function fit (full line) that shows clearly a lower correlation value of $R^2 = 0.98$.

$\Gamma(t) =$

$$p_1 + p_2 \exp\left[-\left(\frac{t - p_3}{p_4}\right) \frac{\left(\frac{t - p_3}{p_4}\right) + (p_5 - 1)}{p_5 - 1}\right]^{p_5 - 1} \quad (10)$$

where p_i represents the fit parameters.

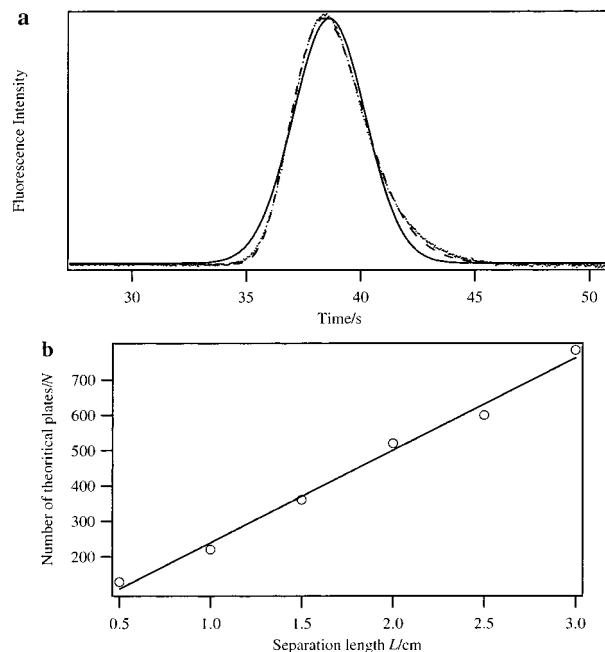


Figure 5. Flow injection analysis at pH 9 for fluorescein in a PET-PE microchip (channels section, $50 \mu\text{m} \times 44 \mu\text{m}$). (a) Experimental detection peaks with Gaussian and asymmetric function peak fits; see text for more details. (b) Variation of the number of theoretical plates as a function of the detection distance L from the injection point.

$\Gamma(t)$ is derived from a Poisson distribution, which is well established in chemical engineering for describing asymmetrical distributions.⁴¹ The asymmetry of the peak can be understood qualitatively when looking at Figure 4b, where it can be seen that a small part of the liquid will be delayed with respect to the average because of the influence of the lamination. This results in the slow tail visible in Figure 5a at higher detection times. All this corroborates the predictions of Andreev et al. concerning the Taylor dispersion effect in composite microchannels.²⁶

In Figure 5b, the number of theoretical plates, N , is presented as a function of the separation length, L . N is calculated with the following relations:

$$N = (t_m / \sigma_m)^2$$

$$t_m = \sum f(t) t \quad (11)$$

$$\sigma_m^2 = \sum f(t) (t - t_m)^2$$

where t_m represents the first momentum of the normalized peak distribution $f(t)$ and σ_m the relative standard deviation of $f(t)$ around t_m . The slope of the linear fit gives a value of $N_L = 2320$ theoretical plates per centimeter or $N_t = 120$ theoretical plates per second for fluorescein (with $N_t = N/t_R$, where $t_R = t_m$, and is the retention time of the analyte). Flow injection analysis on fluorescein performed by Jacobson et al.²⁰ showed that a glass microchip gives about 1600 theoretical plates per second when a separation electric field of 500 V/cm is used. One order of magnitude separates the separation efficiencies of the two chips,

(41) Levenspiel, O. *Chemical Reaction Engineering*, 2nd ed.; J. Wiley: New York, 1972.

which cannot be explained only by the difference in absolute electroosmotic flow between glass and plastic microchannels (lower in plastic channels⁵).

In CE experiments, if effects such as Joule heating or sample–wall interactions are not considered, three principally unavoidable sources of band broadening exist. Namely, dispersion effects during the separation and the effects of both injection and detection govern the upper limit of the separation efficiency. If the separation efficiency is expressed in terms of the theoretical plate height H ($H = L/N$), the resolution of the device is characterized by H_{tot} , given by

$$H_{\text{tot}} = H_{\text{inj}} + H_{\text{det}} + H_{\text{disp}} \quad (12)$$

where H_{inj} , H_{det} , and H_{disp} are the contributions to the plate height from the injection plug, detection path length, and the dispersion effects, respectively. The contributions from the injection plug length and the detection window length are time independent and can be calculated by using eq 13 with the characteristic lengths defined in Figure 2.

$$H_{\text{inj}} = \frac{l_{\text{inj}}^2}{12L} \quad (13)$$

$$H_{\text{det}} = \frac{l_{\text{det}}^2}{12L}$$

The lengths of the injection plug, l_{inj} , and the detector path, l_{det} , are constant for all experiments.

In composite microchannels, the dispersion contribution to the peak broadening can be separated into two terms:²⁶

$$H_{\text{disp}} = H_{\text{diff}} + H_{\text{Taylor}} \quad (14)$$

where H_{diff} is the plate height from axial diffusion and H_{Taylor} is the plate height from Taylor dispersion. The axial diffusion contribution can be calculated by using eq 14:

$$H_{\text{diff}} = \frac{2D}{v_{\text{tot}}} \quad (15)$$

where D is the diffusion coefficient of the analyte in the buffer and v_{tot} is the velocity of the analyte ($v_{\text{tot}} = v_{\text{eo}} + v_{\text{ep}}$), v_{ep} being the electrophoretic velocity of the analyte.

For composite microchannels, the height equivalent to the theoretical plate H_{Taylor} can be calculated using the same theoretical approach as in studies describing peak broadening for a generalized flow profile in field-flow fractionation (FFF).⁴² The calculation is based on the approximation of the 2D velocity profile $v(x,y)$, shown in Figure 4, by the one-dimensional velocity profile $v(y) = v(a/2,y)$.²⁶ For channels that are not much wider than they are deep, as it is the case for our channels, this calculation gives a lower estimate for the influence of the Taylor dispersion, and thus the real H_{Taylor} for our channel will be higher than the calculated one. The formulas for the calculation of the 1D approximation of H are according to Andreev et al.²⁶

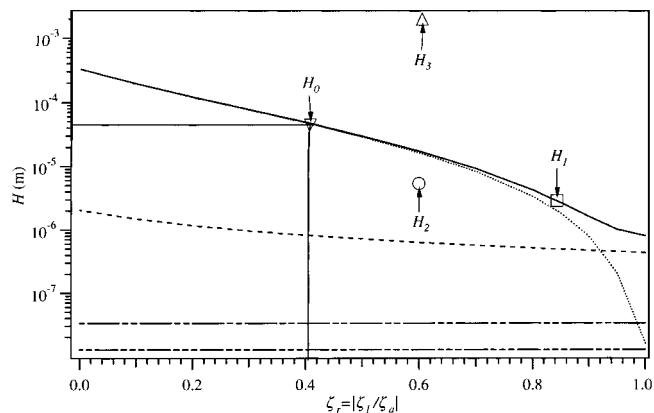


Figure 6. Dependence of height equivalent to theoretical plate H on the absolute value of the ratio of the ζ -potentials of lamination and ablated walls at pH 9 for channels of same cross section. The different contributions are plotted independently on a logarithmic scale: (---) H_{inj} , (-·-·-) H_{det} , (- - -) H_{diff} , (···) H_{Taylor} , and (—) H_{tot} . Parameters: channel section, $50 \mu\text{m} \times 44 \mu\text{m}$; for an electric field of $E = 500 \text{ V cm}^{-1}$, the electroosmotic velocity is $v_{\text{eo}} = 22 \times 10^{-2} \text{ cm s}^{-1}$; for fluorescein the electrophoretic velocity is $v_{\text{ep}} = -16.8 \times 10^{-2} \text{ cm s}^{-1}$ and the diffusion coefficient $D = 3.4 \times 10^{-6} \text{ cm}^2 \text{ s}^{-1}$. The different H_i (markers) represent respectively the theoretical plate, H_0 , calculated from the experimental value obtained with the PET–PE microchip shown in Figure 5a (inverted triangle marker); the theoretical plate, H_1 , obtained by Jacobson et al.²⁰ (square marker); the simulated value, H_2 , for the PC–PE microchip using the mathematical model given in eqs 15 to 19 (round marker); and the theoretical plate, H_3 , of the microchip composed of ablated PC and a lamination polymer, which have the same ζ -potential as PE but are opposite in sign (triangle marker).

$$H_{\text{Taylor}} = \chi \frac{b^2 v_{\text{av}}^{1d}}{D} \quad (16)$$

where

$$v_{\text{av}}^{1d} = \frac{1}{b} \int_0^b v(y) dy \quad (17)$$

is the average of the velocity profile $v_{\text{eo}}(a/2,y)$, and χ is defined by eq 18:

$$\chi = \frac{1/b}{4v_{\text{tot}}v_{\text{av}}^{1d}} \int_0^b B^2(y) dy \quad (18)$$

with

$$B(y) = \frac{1}{b} \int_0^y [v_{\text{av}}^{1d} - v(y')] dy' \quad (19)$$

The different integrals (16), (17), and (18) are calculated by using the procedure described in the Theory section.

In Figure 6, the different theoretical plate heights H_i are plotted on a logarithmic scale as a function of the ratio $\zeta_r = \zeta_l/\zeta_a$. The channel dimensions, a and b , as well as the ζ -potential of the ablated surface, ζ_a , are kept constant, while the ζ -potential of the lamination wall, ζ_l , is varied in the range from 0 to ζ_a . The dispersion due to the axial diffusion, H_{diff} , increases with decreasing ζ_r -ratio, because when the electroosmotic velocity is reduced

(42) Martin, M.; Giddings, C. J. *J. Phys. Chem.* **1981**, *85*, 727–733.

by lower values of ζ_i , the retention time increases, leading to a longer diffusion time. The Taylor dispersion, H_{Taylor} , increases as well with decreasing ζ_r , and it is minimal when the composite microchannel approaches a homogeneous channel ($\zeta_r = 1$). For ζ_r -ratios of $\zeta_r \geq 0.92$, the peak broadening is dominated by axial diffusion and the constant contributions of the injection and detection parts (eq 12). For ζ_r -ratios of $\zeta_r < 0.92$, Taylor dispersion overcomes the axial diffusion dispersion, and for $\zeta_r = 0.7$, the separation efficiency of the column is completely dominated by the Taylor dispersion, i.e., $H_{\text{tot}} = H_{\text{Taylor}}$. When the Taylor dispersion is maximal, $\zeta_r = 0$, the Taylor theoretical height, H_{Taylor} , is 2 orders of magnitude higher than in the case where only diffusion, injection, and detection broadening are considered. If we neglect the difference in pH and compare these results with those from experiments carried out between measurement and calculation at $\zeta_r = 0.38$, which corresponds to the ζ_r -ratio of PET-PE microchannels based on our EOF measurements (see Table 1), the Taylor dispersion is 1 order of magnitude higher than the other contributions.

Moreover, by reporting the theoretical plate height of fluorescein $H_0 = 44 \mu\text{m}$ at pH 9 (inverted triangle marker in Figure 6), measured from Figure 5a, in the graph of Figure 6, we obtain a ζ_r -ratio of $\zeta_r \approx 0.40$, which is in very good agreement (less than 5% of difference) with the ζ_r -ratio estimated by electroosmotic measurements at pH 4.6 and the resulting fits shown in Table 1 (right part for PE-PET microchannels). This proves that the ζ_r -ratios are equal at pH 4.6 and pH 9 for PE-PET channels. Thus, the separation efficiency in our PE-PET microchannels is governed mainly by Taylor dispersion. Comparatively, the theoretical plate reported by Jacobson et al.,²⁰ $H_1 = 2.85 \mu\text{m}$ (square marker in Figure 6), is plotted on the theoretical curve (H_{tot}) of Figure 6. As expected, the PET-PE microchip gives a theoretical plate, H_0 , 1 order of magnitude higher than H_1 , confirming that the efficiency in a composite microchip with a low ζ_r -ratio is restricted by the Taylor dispersion. However, the value H_1 corresponds in the theoretical curve of the Figure 6 to a ζ_r -ratio different from unity. This may explain also the trailing edge of the peak shape observed by Jacobson et al.²⁰

In the case of the PC-PE microchip, the theoretical plate, H_2 (round marker in Figure 6), has been estimated by using the ζ -potential values listed in Table 1 (right part) and the mathematical model described by eqs 15–19. For an equivalent ζ_r -ratio, the value of H_2 is smaller than the theoretical value (full line in Figure 6) estimated for PET-PE. This results from the lower electro-

osmotic velocity in PC-PE microchannels than in PET-PE (see Figure 3). In fact, the Taylor dispersion expressed by eq 16 is proportional to the velocity. Therefore, the ζ -ratio is not the only parameter controlling the Taylor dispersion; the electroosmotic velocity and the relative sign of the ζ -potential of the materials forming the composite microchip are also important parameters. Using the same procedure to calculate H_2 , we simulate the dispersion expressed by a microchip, with the same ζ_r -ratio as for PC-PE but with a ζ -potential of the PC different in sign from that of PE. The value H_3 is reported in Figure 6 (triangle marker), underlying the effect of dispersion expressed by such a kind of system. Hence, precise knowledge of the ζ -potentials of the materials composing the capillary walls, as presented in this contribution, is of major importance for understanding μ -CE experiments. It would be interesting to study how coating methods^{43,44} can reduce the disparity between the ζ -potentials when using the μ -CE system.

CONCLUSION

This work demonstrates that the electroosmotic flow in composite microchannels, with nonequal ζ -potentials, depends on the relative channel dimensions. Combining the theoretical modeling, eqs 2 and 6, with experimental data allows the determination of the individual ζ -potentials of each material. Further, a simple linear combination of the Smoluchowski equation predicts the EOF in such channels, if the ratio e/f ranges from 0.22 to 0.44. Finally, a flow injection analysis reveals that the nonuniformity of the electroosmotic flow due to nonequal ζ -potentials leads to a strong Taylor dispersion and decreases the efficiency of capillary electrophoresis in composite PET-PE microchannels. If the ζ_r -ratio reaches below a certain value ($\zeta_r < 0.7$ for the given channel section), the peak broadening is dominated by Taylor dispersion, and the theoretical plate height, H , can increase up to 2 orders of magnitude. To avoid this poor separation efficiency, postchemical or postphysical treatments homogenizing the ζ -potentials in the composite microchannels have to be considered for applications in microseparations capillary zone electrophoresis.

ACKNOWLEDGMENT

F.B. and F.W. thank l'Ecole Polytechnique Fédérale de Lausanne (EPFL) for a doctoral fellowship. We thank Brian Senior for the SEM picture and the workers in our electronic workshop, especially F. Troillet, for all the electronic support for HV handling and homemade instruments.

Received for review September 19, 2000. Accepted November 29, 2000.

AC0011181

(43) Wang, Y.; Dubin, P. L. *Anal. Chem.* **1999**, *71*, 3463–3468.

(44) Barker, S. R. L.; Tarlov, M. J.; Branham, M.; Xu, J.; MacCrehan, W.; Gaitan, M.; Locascio, L. E. In *Micro Total Analysis Systems 2000*; van den Berg, A., Olthuis, W., Bergveld, P., Eds.; Kluwer Academic Publishers: Dordrecht/Boston/London, 2000; pp 67–70.